

## **Three dimensional reservoir geological model and multiple scenario volumetrics of the F23 Miocene carbonate build-up, Luconia Province, offshore Sarawak**

VOLKER C. VAHRENKAMP, YUSOFF KAMARI AND SYED ABD. RAHMAN

EPG-PRO, Sarawak Shell Berhad  
Locked Bag #1  
98009 Miri  
Sarawak

**Abstract:** Typically, the geology and production behavior of gas reservoirs in the atoll shaped Miocene carbonate structures of the Central Luconia province, offshore Sarawak, are best constrained in the center of the field due to a biased distribution of wells. Control over the reservoir architecture, pore volume and fluid flow behavior decrease significantly towards the reservoir flanks introducing uncertainties for an optimized reservoir management. An integrated reservoir geological study was initiated with the objective to decrease uncertainties and increase the understanding of their impact on static and dynamic reservoir models. Data from an integrated core, seismic and petrophysical evaluation, including lateral seismic porosity prediction and the application of geostatistics, were combined to a 3-D fully computerized reservoir model. The core and seismic evaluation reveals a complex internal reservoir architecture strongly influenced by paleo-wind pattern and sea-level fluctuations with backstepping, progradational and aggradational growth phases. Transgressive systems tracts are represented by dense argillaceous limestones, which form more or less continuous blankets possibly isolating gas volumes and influencing vertical water movement. During repeated periods of flooding the platform back-stepped up-wind only to prograde down-wind again during sea-level high stands until re-reaching the previous platform margin.

An uncertainty tree was constructed for the F23 field in order to assess the impact of combined and individual uncertainties on static and dynamic reservoir models. Parameters considered in the uncertainty tree are the top carbonate structure, the porosity distribution, the hydrocarbon saturation and the gas expansion factor. Most likely, low and high cases were used in order to assess the parameters with the most impact on the uncertainty of hydrocarbon volume and fluid flow, in particular possible flank water encroachment. Results from the volumetric calculations arrive at a most likely GIIP close to that derived from material balance analysis. However, low and high cases significantly exceed the uncertainty range of the material balance GIIP. While the geology of the reservoir flank is now better constrained using refined seismic interpretations, uncertainties in these areas remain high.

### **INTRODUCTION**

The F23 structure is a Middle Miocene steep-flanked carbonate platform, slightly elongated in a NNE-SSW direction measuring some 4.5 by 7.5 km in size (Fig. 1). It is one of the major gas fields of the Central Luconia province and by 6/96 has produced some 40% of its GIIP from 11 producing wells since coming on stream in 1983. An extensive data set exists which is based on 14 wells (3 cored), 2D seismic coverage of different vintage and quality and 13 years of cumulative production data. However, despite a number of reservoir geological evaluations large uncertainties remain in the geological model and static volume estimates of hydrocarbons in place differ significantly from performance based estimates. Probably because

many factors influence the uncertainty range of the static hydrocarbon volume, their individual contribution to the overall uncertainty has not been weighed or made transparent in former reservoir geological evaluations. It is thus difficult to assess whether the static reservoir model can contribute to better estimates of the hydrocarbon volume and whether the acquisition of new data can help to narrow uncertainties and if yes by how much (value of information).

New insights into the reservoir architecture and the porosity and saturation distributions from a core/log/seismic review and a lateral porosity prediction study have altered the perception of the reservoir architecture and thus warrant a revision of the reservoir geological model and a reevaluation of static reservoir volumes.

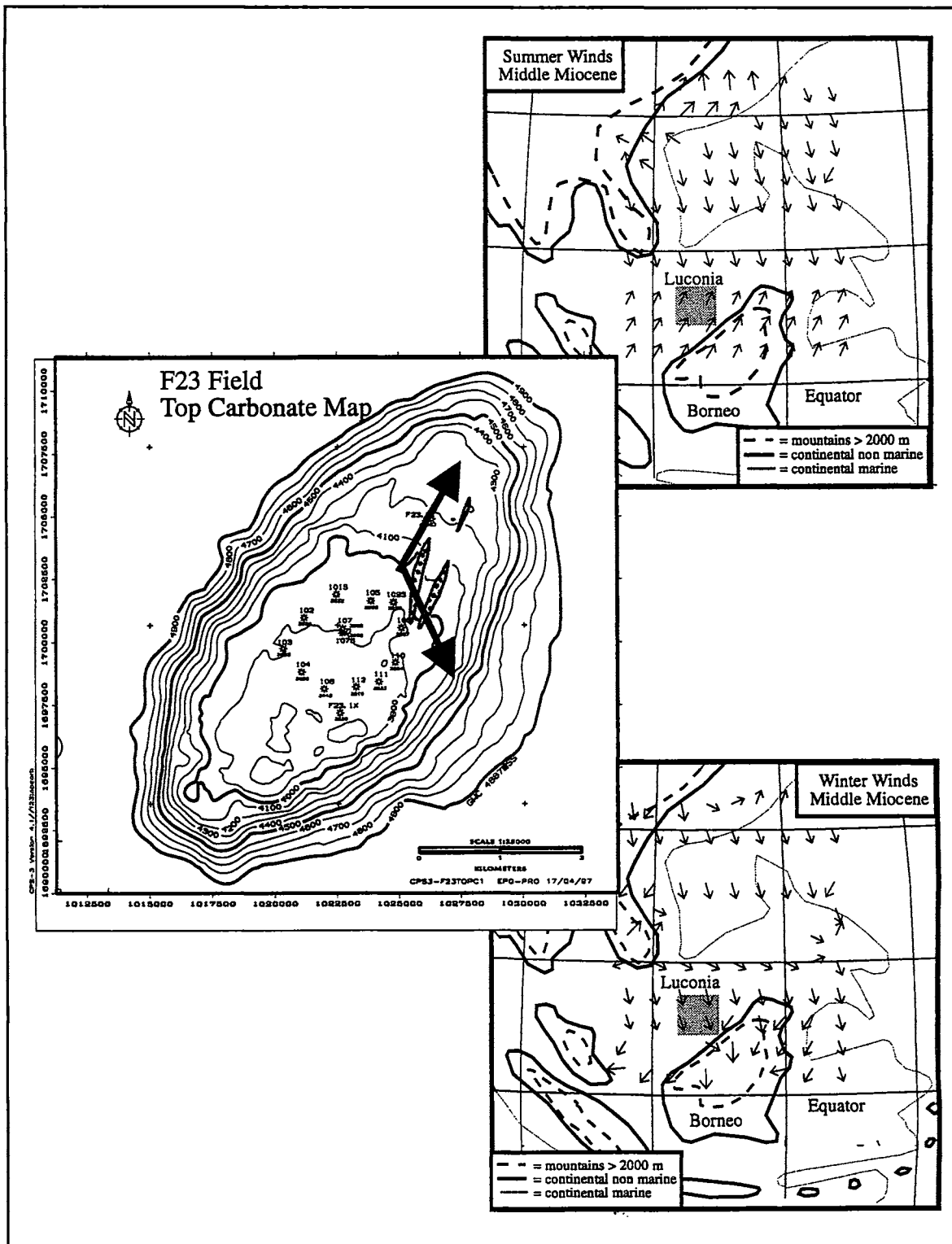


**Figure 1.** The F23 reservoir is located some 178 km offshore Bintulu, Sarawak, in the center of the Luconia Province. The carbonate structure has steeply dipping flanks at its SE to NW side. The NW to SE margin is bulging and more gently dipping. This bearing coincides with the downwind direction of Miocene paleo winds (see seasonal wind maps).

## PROJECT OBJECTIVES

The newest results were integrated from a core and seismic review, a lateral porosity prediction study and improved hydrocarbon saturation functions in order to:

- revise and update the reservoir geological model, in particular with respect to the flanks of the field;
- update estimates of static reservoir volumes using computerized 3D reservoir models;
- assess the impact of the most important individual parameters on volume estimates using a multiple scenario uncertainty assessment.

## DATA AND TOOLS

The revised geological model and volume assessment are based on

- a paleo-wind direction map for the Middle Miocene of the South China Sea derived from computer simulation;
- the evaluation of 1,891 ft of core from wells F23-1, F23-2 and F23-107 & 107s;
- the determination of depositional stratigraphy using strontium isotopes (Vahrenkamp, 1996);
- the evaluation of seismic reflectivity and impedance patterns on 8 seismic lines;
- a 2D lateral porosity prediction study on 8 seismic lines using the Hampson Russell inversion software;
- a geostatistical evaluation of well and impedance derived porosity values using Isatis software;
- the establishment of porosity-dependent saturation height functions as derived from log data and
- a top structure map derived from a 2D seismic grid;
- fully computerized 3D reservoir modelling using Shell GEOCAP software.

## GEOLOGICAL REVIEW

### Overall Setting: Miocene Winds over the Luconia Province

A climate simulation model predicts two principle wind directions over the Luconia area during the Middle Miocene (Fig. 1). Apparently, winter and summer winds were not in opposite directions as observed in the monsoonal patterns of the present but rather perpendicular to each other with Southwesterlies during the summer and Northwesterlies during the winter. Numerous

studies have revealed the influence of wind on carbonate platform architecture and the distribution of sediments within platforms (Hine and Neumann, 1977; Eberli and Ginsburg, 1989). Generally, windward margins are found to be steep and reef rimmed, while leeward margins are more gently dipping and the location of platform progradation due to the downwind deposition of winnowed carbonate particles. A comparison of the overall shape of platform F23 with growth patterns expected from paleowind directions shows excellent agreement (Fig. 1). Steep platform margins occur at the presumably windward sides from (clockwise) the SE to the NW while more gently dipping margins coincide with the presumably leeward sides from the NE to the SE. Thus, while the overall elongated shape of the platform is probably related to an older structural pattern of the Luconia province, the internal platform architecture and distribution of sediments is most likely a result of paleo-winds.

### Core Review

A review of all available core material reveals that meter-scale shallowing upwards cycles form the principle building blocks of all F23 cores. An ideal small scale shallowing upwards cycle consists of:

- a reflooding lag layer (coarse grainstones, massive head coral debris, rhodolites).
- a condensed maximum flooding section (dense, argillaceous, sometimes dolomitic packstone/grainstone).
- an aggradational section: coarsening upwards pack/grainstone with finger corals in the low parts and more massive corals in the upper part of the section).
- an exposure horizon.

Small scale cycles are stacked into large cycles which essentially coincide with zones one four previously differentiated in the F23 platform based on large scale seismic reflector pattern (Fig. 2). Overall, large-scale cycles have similar shallowing upward trends found in small-scale cycles. The lower part of the cycle consists of relatively thin small-scale cycles with pronounced evidence for flooding and deeper water deposition and less pronounced shallow water sections. They are superseded by small scale cycles with thick shallowing upwards sections. The upper parts of the larger cycles have only little deeper water sediments and consist mainly of relatively thin, shallower water small-scale cycles with ample evidence for subareal exposure. Paleo-environmental conditions caused a lateral differentiation in the upper two large-scale cycles (zones 1 and 2) with the distribution of reefal and

lagoonal facies in the up-wind part of the platform and open marine deposits in the down wind direction.

## Seismic Review

### Top Carbonate

The top structure map has been derived from a grid of 2D seismic data. The estimated error based on the time/depth conversion and the pick uncertainty is quoted as  $\pm 50$  ft at the top reservoir and  $\pm 120$  ft at the base of the flanks.

### Faulting

Only few minor faults have been mapped. However, evidence exists from seismic lines that small scale faulting may be more common. This is thought to have an advantages effect on reservoir connectivity (see discussion below).

## Seismic Reservoir Architecture

The previous atoll-type reservoir model was based mainly on the recognition of three more or less parallel reflectors on seismic lines that were used to differentiate zones 1 to 4 of the reservoir model (Fig. 2a). The sediment packages between the reflectors were believed to be the layercake infill of a reef-rimmed lagoon with vertical lithology variations related to phases of shallow or deeper water depth during deposition. However, a closer look at seismic reflection and impedance sections reveals some additional inclined reflectors between those reflectors, which define the major growth packages of zones 1 to 4 (Fig. 2b). The additional reflectors are less well defined and slope down-wind towards the Northeast. A correlation of cores, logs and synthetic seismic with seismic sections reveals that most hard reflectors are caused by relatively dense rock sections which were deposited

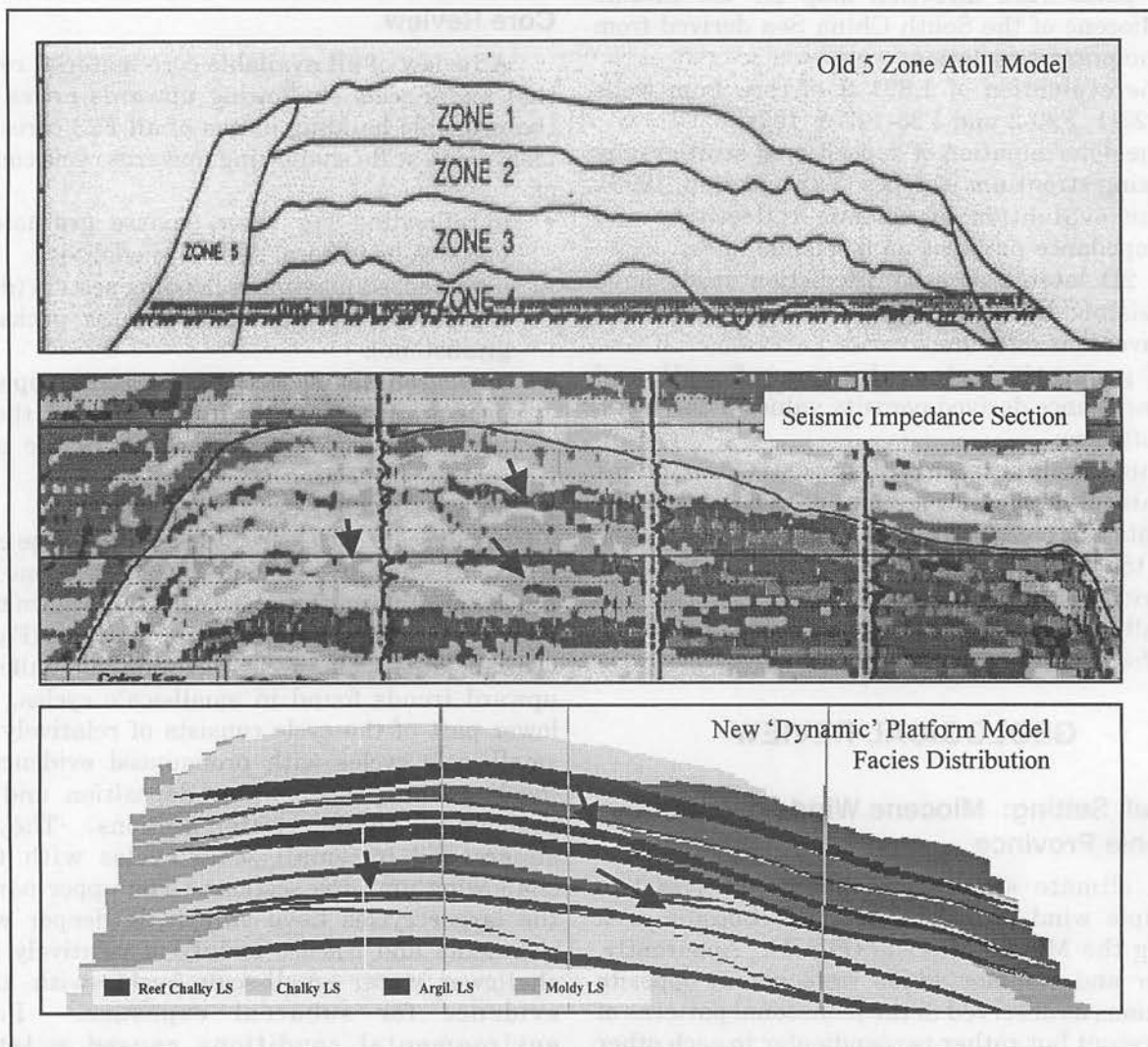


**Figure 2.** A comparison of 3 SW to NE sections through F23 field: the previous reservoir model, a seismic impedance line and a 3D computer realization of the new geological model. Note in the new model the preservation of clinofolds (arrows) visible on the seismic section.

after platform exposure during reflooding in relatively deep water. Based on the seismic signal the flooding units are laterally extensive and well correlateable across the platform. The inclined reflectors are interpreted to be clinoforms of a prograding depositional system. The clinoform are best developed in a Northeasterly direction and less apparent on Northwest/Southeast lines. Thus, either the Southwesterly summer winds dominated sediment transport in F23 compared to the Northwesterly winter winds or, alternatively, seismic lines give a better resolution along the elongated Southwest/Northeast axis of the field.

## GEOLOGICAL MODEL

### Architecture

Age dating, paleo-climate modelling, the lateral variation of facies described in cores and the recognition of clinoforms on seismic sections all cast doubt on a simple layercake depositional model as proposed previously. Instead the evidence points towards a more dynamic depositional system with a backstepping, aggradational and progradational platform growth style driven by the combined effects of at least three orders of sea-level fluctuations.

The overall backstepping geometry of the more than 1,500 feet thick platform and its ultimate demise is related to the second order sea-level fall at the end of the Middle Miocene (TB2) (Vahrenkamp, 1996; Haq *et al.*, 1988). Reservoir zones 1 to 4 form the main reservoir units. These several hundred feet thick packages, which are in turn build by small-scale cycles and are separated by pronounced exposure horizons overlain by major flooding zones, were probably deposited during third order sea-level cycles of the Middle Miocene with this architectural blueprint:

Following the exposure of the previous sequence, the actively growing part of the platform backstepped to an up-wind position during flooding. Here, it first aggraded to reach the sea-level and then prograded during sea-level high stands downwind until reaching the platform margin giving rise to clinoform growth patterns. The final growth stage consists of a flat-topped, reef and/or sand shoal rimmed platform with an extensive lagoon which covers most of the platform. This pattern is fully developed in zone 3 and probably in the incompletely drilled zone 4. During deposition of zones 2 and 1 the growth potential of the platform had deteriorated to the point that thick packages of winnowed sands and debris were deposited downwind in a deeper water fore reef depositional environment. Shallow water lagoonal conditions were limited to the up-wind part of the platform

and did not have enough time to prograde back to the down-wind platform margin. During the final growth stage the area of shallow water deposition never expanded beyond a small west/central part of the platform.

### Lithology and Porosity Systems

Three lithologies are differentiated based on their porosity system. This simple pore type based subdivision is advantageous because it can be recognized in the seismic properties of the reservoir rock and thus allows the incorporation of porosity data from a lateral porosity prediction based on seismic impedance.

*Chalky Lithology* is defined based on microscopic pore characteristics as a rock with connected interparticle porosity, which may also contain intraparticle, moldic porosity, if it is connected to the interparticle porosity. With decreasing absolute porosity connectedness of the pore system is lost and it grades into the tight lithology class. The seismic impedance of this lithology is higher compared to that of moldic lithology for relatively high porosities but similar for relatively low porosities.

*Moldic Lithology* is defined based on microscopic pore characteristics as a rock with intraparticle, fossil- or grain-moldic porosity with cemented interparticle space. While in an extreme case porosity could be unconnected this has not been observed in F23. Instead, porosity is connected albeit with a permeability usually less compared to chalky lithologies with equal porosity. In sections with very high moldic porosity pores become progressively connected and the properties of the rock grade into that of chalky lithologies. At decreasing porosity moldic lithologies form a continuum with tight lithologies.

*Tight Lithology* is a collective term for reservoir rock with low porosity and permeability. This may be rocks with low-end chalky and moldic pore systems as well as tight argillaceous limestones and dolomites.

### Intra-platform Pore Type Distribution

Pore types are closely associated with depositional facies (Fig. 2c). Chalky lithologies occur in reefal and lagoonal shallow water limestones and are often associated with intense diagenetic leaching at exposure horizons. Moldic lithologies are usually associated with well-cemented fore-reef grainstones and packstones. Tight lithologies are found in the transgressive flooding units and in condensed sections associated with maximum flooding units. Applying this general association to the distribution of lithofacies in the multi-cyclic architecture of the carbonate platform

helps to predict vertical and lateral changes in the porosity distribution of the reservoir away from well control.

The potentially most important aspect is the distribution of tight units in the reservoir. Transgressive systems tracts are usually composed of tight argillaceous limestones, which based on seismic evidence form a more or less continuous blanket across the platform and may influence vertical water movement and in an extreme case isolate gas volumes. Tight argillaceous layers are present in the major transgressive units separating the reservoir zones 1 to 4 as well as in the minor transgressive units of the prograding clinoforms that can be differentiated on seismic lines. Whether these units really impede the flow of gas is unclear. It depends on the presence of depositional/erosional gaps, the presence and throw of faults, the presence and frequency of fractures and whether the permeability is small enough to prevent gas flow considering the large areal extent of the low permeability layers. However, the impact of these features on fluid flow can now be assessed, by exporting the computerized 3D reservoir geological model into a reservoir simulator in the integrated Shell GEOCAP/MORES computing environment. Furthermore, it can be deduced that the highest reservoir permeabilities are to be expected in the upwind and central part of the platform with decreasing permeabilities downwind. This point is validated by well data from F23 and other Luconia fields.

### Qualification of 3D Porosity Data

Porosity values used for the 3D reservoir geological model are based on core and log data and a study of lateral seismic impedance variations. The seismic study utilized a set of eight 2D seismic lines. Well calibrated lateral impedance predictions were done using Hampson-Russel software. 2D seismic impedance sections reveal significant lateral and vertical impedance variations (Fig. 2b), which can be translated into porosity variations using well derived impedance/porosity cross plots. However, even though seismic velocity in a homogeneous material is assumed to change linearly as a function of porosity, cross plotted impedance/porosity data from wells F23-1 & 2 have a large spread and do not very well describe a linear trend. Yet, if the data is subdivided into chalky and moldic/tight lithology types, two acceptable linear impedance/porosity trends can be differentiated and approximated by straight lines. The derivation of porosity values from impedance sections thus requires the subdivision of the reservoir into intervals of distinct lithology. Based on core data, seismic patterns and the sequence stratigraphic

interpretation the reservoir section of F3 has been subdivision into 9 distinct lithology units for which porosity data were derived from seismic impedance sections and lithology specific impedance/porosity correlations.

Since the porosities derived from impedance are data points along a set of 2D seismic lines, seismic porosity grids were kriged and then used as a external drift for the kriging of well porosities to derive the final porosity maps for the nine lithology units (Rahman and Vahrenkamp, 1996). Minimum and maximum porosity maps were derived assuming three standard deviations from the mean case. This covers the theoretical range of uncertainty assuming normally distributed and independent errors.

### Saturation

Different lithofacies of Central Luconia carbonates have different capillary behavior. For the spatial modeling of saturation one would ideally like to derive these lithofacies types from open hole logs and apply lithofacies type specific saturation-height functions that are measured on core plugs. However, as an alternative saturation/height functions were derived from log derived saturation profiles using geological marker as well as porosity classes to discriminate distinct groups of saturation/height functions.

### Permeability

Porosity/permeability correlations were derived from data of wells F23-1 & 2 using the subdivision of the section into the three lithologies and their respective log calculated and core calibrated porosity and permeability data. The porosity/permeability functions are then established using a line fitting option in the Shell petrophysical computer program LOGIC.

## 3D GEOLOGICAL COMPUTER MODEL

Reservoir models were constructed with the integrated log correlation and 3D reservoir geological modeling program GEOCAP. First, time slices and lithologies were correlated with the aid of the well-correlation sub-program GEOLOGIX. Subsequently, data were transferred to MONARCH, modeled and manipulated to yield 3-D models of lithofacies, porosity, hydrocarbon and permeability distribution.

### Model Preparation

All 14 wells of the field and in addition some 24 control points (pseudo wells) fringing the field were correlated in GEOLOGIX. The datum level for palinspastic reconstruction is the sequence boundary at the top of zone 3 which is thought to

have formed a more or less level layer at the time of formation. The information entered consists of:

- the carbonate reservoir interval;
- the tops and bottoms of the major time slices as determined from seismic and well data (zones 1 to 4);
- the tops and bottoms of subordinate time slices.

The 3 lithofacies distinguished in the core study were correlated based on juxtaposition in neighbouring wells and the underlying sequence stratigraphic model. A fourth undrilled lithofacies, flank reefs, was introduced to maintain the option for later studies to test various reservoir properties for the flanks of the field with reservoir simulations. However, in the MONARCH runs used for the static reservoir model the properties of the reef and chalky lithologies were interpreted to be identical.

Even though the growth patterns of the platform follow the same principles in each deposition cycle similar lithofacies from different cycles may have different properties because of a different diagenetic history of each cycle. In order to maintain the flexibility to address such property differences in

the model each lithofacies was marked based on the larger cycle scheme. Thus 12 lithofacies are differentiated in the model (zones 1 and 2 contain all 4 lithofacies, zone 3 contains the chalky, reef and tight lithofacies and zone 4 the chalky lithofacies only).

### Model Size

The model size includes the complete carbonate build-up structure with a rectangular area of 4.75 km x 7.2 km rotated with its length axis 40 degrees from North to the East (Fig. 3). The maximum thickness of the modelled sequence is some 1,200 feet. MONARCH uses a matrix of discrete volume cells (voxels) to model the distribution of lithofacies, properties and fluids within the modeled volume. In this study the voxel size is 2 feet by 100 m by 100 m. Consequently the full MONARCH model contains approximately  $2.1 \times 10^6$  voxels. The top of the model volume lies within the shales, which overlie the carbonates and provide the seal for the reservoir; the bottom is defined by a plane some 115 feet below the GWC.

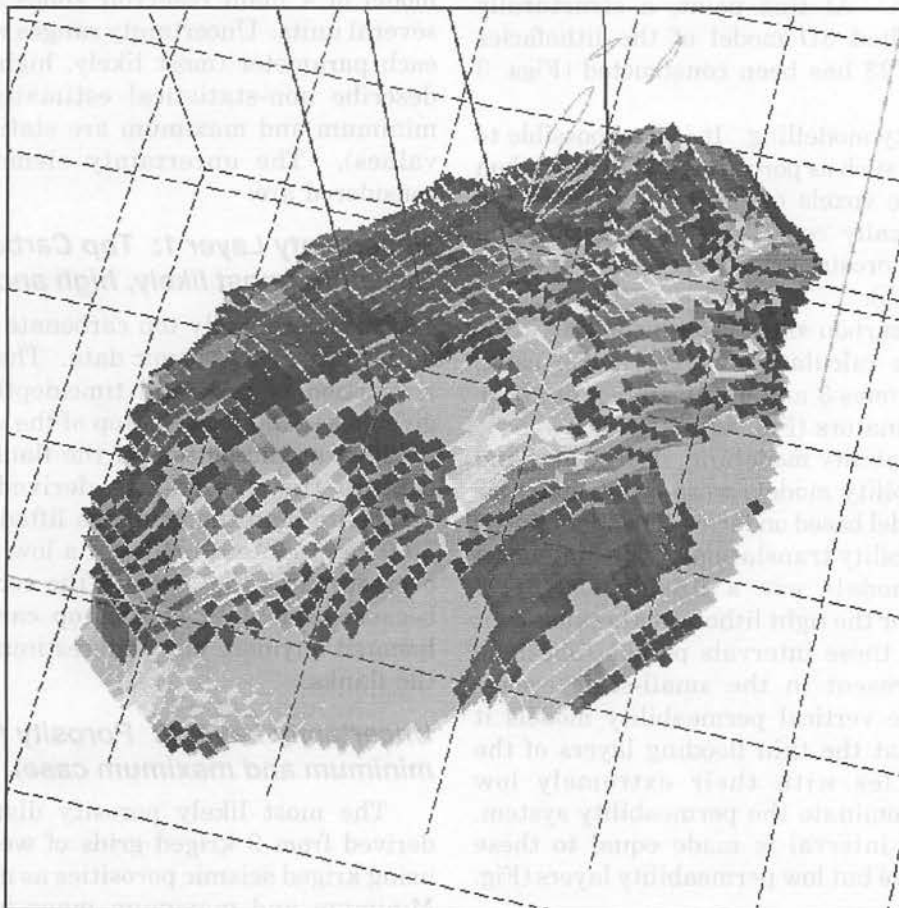


**Figure 3.** View of the structurally constrained 3D computer model of the facies distribution in F23 field. A surface square is 1 km<sup>2</sup> in dimension. The model contains  $2.1 \times 10^6$  volume cells (voxels) with an individual size of 100 m x 100 m x 2 ft. Lines entering the model are wells.

## Model Construction

**Stage 1:** Modelling of correlated lithofacies. The first stage of the modelling involves the 3D mapping of all bodies defined in the GEOLOGIX correlation exercise. The bodies are mapped using a kriging algorithm. At this point in the modelling exercise bodies are laterally unconstrained and extend to the outer limits of the model area.

**Stage 2:** Modelling of the present-day structural deformation. In order to transfer the model into the present day structural domain the datum was deformed using the top zone 3 depth contour map derived from seismic interpretation. A CPS-3 map was transferred via the DSI sub-program into a GEOCAP grid map. A structurally constrained 3-D MONARCH model results.

**Stage 3:** Incorporation of faults. Several small faults, which were mapped in the seismic interpretation exercise, were imported into the MONARCH model.

**Stage 4:** Model extent. In order to limit the model to the extent of the carbonate platform the lithobodies are clipped against the top carbonate grid, which has been imported from CPS-3 via the DSI subprogram. At this point, a structurally constrained, faulted 3D model of the lithofacies distribution in F23 has been constructed (Figs. 3 and 4a).

**Stage 5:** Porosity modelling. It is now possible to assign properties such as porosities and hydrocarbon saturation to the voxels of the lithofacies model. Nine geostatistically constrained lithofacies and zone dependent porosity grids were assigned to the 3D model (Fig. 4b).

**Stage 6:** Hydrocarbon saturation modelling. Gas saturations were calculated for each voxel using porosity and in zones 3 and 4 as well height above FWL as discriminators (Fig. 4c).

**Stage 7:** Permeability modelling. Horizontal and vertical permeability models were constructed for each porosity model based on facies dependent linear porosity/permeability translations. The horizontal permeability models use a linear poro/perm transformation for the tight lithofacies because over the thickness of these intervals porous limestone intervals are present in the small-scale cycles. However, for the vertical permeability models it was assumed that the thin flooding layers of the small-scale cycles with their extremely low permeabilities dominate the permeability system. Thus the whole interval is made equal to these laterally extensive but low permeability layers (Fig. 4d).

## 3D Model Summary

At the end of the modelling exercise the following 19 MONARCH models have been

constructed:

- a model of the most likely geological facies distribution (one facies model);
- a model of the expectation, minimum and maximum porosity distribution as a function of lithofacies and depositional cycle which is based on well and seismic porosity data (3 porosity models);
- a model of the most likely, the high and the low hydrocarbon saturation as a function of porosity and height above FWL for each porosity scenario (9 saturation models).
- a model each of the most likely horizontal and vertical permeability distribution as a function of the most likely, the high and the low porosity (6 permeability models).

## GAS VOLUME ESTIMATES USING AN UNCERTAINTY TREE

In order to compute the hydrocarbon volume in F23 an uncertainty tree was constructed with 4 uncertainty layers (Fig. 4). The tree is based on a sequence stratigraphically constrained geological model of 4 main reservoir zones subdivided into several units. Uncertainty ranges were attached to each parameter (most likely, high and low cases describe non-statistical estimates, expectation, minimum and maximum are statistically derived values). The uncertainty elements that were considered are:

### **Uncertainty Layer 1: Top Carbonate Structure (most likely, high and low case)**

The most likely top carbonate map (Fig. 1) is derived from 2D seismic data. The uncertainty as a function of pick and time/depth conversion is given as +/- 50 ft at the top of the structure and +/- 120 ft at the bottom of the flanks. In order to capture the uncertainty derived from the top carbonate map the grid was lifted/lowered by +/- 50 ft to produce a high and a low grid map. This overestimates the error in the center of the field because well data of the top carbonate are not honored anymore but underestimates the error at the flanks.

### **Uncertainty Layer 2: Porosity (expectation, minimum and maximum case)**

The most likely porosity distributions were derived from 9 kriged grids of well porosity data using kriged seismic porosities as an external drift. Minimum and maximum maps were derived by assuming three standard deviations from the mean case, thus covering the theoretical range of data assuming normally distributed and independent errors.



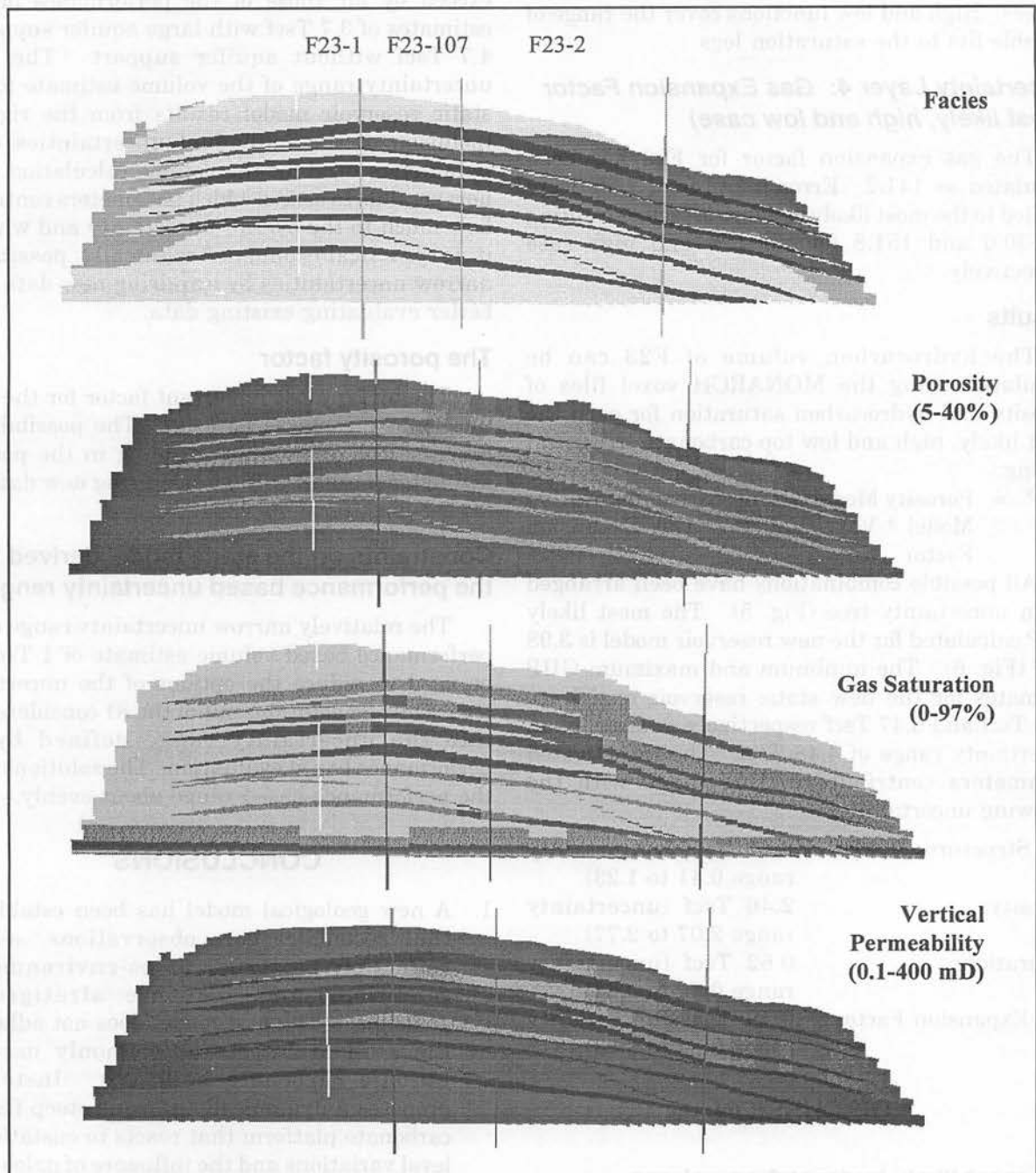


**Figure 4.** SW to NE sections through 3D computerized models of facies and reservoir properties ( $\phi$ ,  $k$ ,  $sh$ ) of F23 field. Note the preservation of geological detail such as clinoforms and up-wind/down-wind architecture.

### **Uncertainty Layer 3: Hydrocarbon Saturation (most likely, high and low case)**

Porosity and height-above-reference-level dependent saturation functions are derived from optimised visual fits to calculated saturation logs split into 6 porosity classes and 2 independent zone classes. High and low functions cover the range of possible fits to the saturation logs.

### **Uncertainty Layer 4: Gas Expansion Factor (most likely, high and low case)**

The gas expansion factor for F23 has been calculated as 141.2. Error margins of 7.5% were applied to the most likely expansion factor resulting in 130.6 and 151.8 for the low and high case respectively.

## **Results**

The hydrocarbon volume of F23 can be calculated using the MONARCH voxel files of porosity and hydrocarbon saturation for each the most likely, high and low top carbonate structural setting:

$$\text{GIIP} = \text{Porosity Model} * \text{Hydrocarbon Saturation Model} * \text{Voxel Volume} * \text{Gas Expansion Factor}$$

All possible combinations have been arranged in an uncertainty tree (Fig. 5). The most likely GIIP calculated for the new reservoir model is 3.98 Tscf (Fig. 6). The minimum and maximum GIIP estimates for the new static reservoir model are 1.99 Tscf and 6.47 Tscf respectively, indicating an uncertainty range of 4.48 Tscf. The investigated parameters contribute to this range with the following uncertainties:

Top Structure:	0.81 Tscf (uncertainty range 0.41 to 1.23)
Porosity:	2.46 Tscf (uncertainty range 2.07 to 2.77)
Saturation:	0.62 Tscf (uncertainty range 0.60 to 0.64)
Gas Expansion Factor:	0.59 Tscf (uncertainty range 0.32 to 0.83)

## **DISCUSSION**

### **The most likely hydrocarbon volume estimate**

The most likely hydrocarbon volume estimate of 3.98 Tscf for the new reservoir model essentially reconciles static and performance based most likely GIIP estimates. The upwards change in the static estimate is linked to changes in the newly derived porosity and hydrocarbon saturation distributions since the same most likely top carbonate structure

map and gas expansion factor were used for estimates derived from the old model.

### **Uncertainty range**

The minimum and maximum estimates of the new model of 1.99 Tscf and 6.47 Tscf, respectively exceed by far those of the performance derived estimates of 3.7 Tscf with large aquifer support to 4.7 Tscf without aquifer support. The large uncertainty range of the volume estimate for the static reservoir model results from the rigorous inclusion of the individual uncertainties of all parameters used for the volume calculation. It is now possible to assess which parameters contribute how much to the overall uncertainty and whether it is practical/economic/technically possible to narrow uncertainties by acquiring new data or by better evaluating existing data.

### **The porosity factor**

The by far most important factor for the large uncertainty range is porosity. The possibility to decrease the uncertainty residing in the porosity estimates is small without acquiring new data (i.e. 3D seismic).

### **Constraints on the static model derived from the performance based uncertainty range**

The relatively narrow uncertainty range of the performance based volume estimate of 1 Tscf can be used to reduce the options of the uncertainty tree. Only 22 solutions out of the 81 considered fall into the uncertainty range defined by the performance based evaluation. The solutions cover the performance-based range about evenly.

## **CONCLUSIONS**

1. A new geological model has been established that reconciles core observations, seismic reflection patterns, paleo-environmental conditions and sequence stratigraphic principles. The new model does not adhere to the atoll architecture commonly used for Luconia carbonate build-ups. Instead it proposes a dynamically growing steep flanked carbonate platform that reacts to eustatic sea-level variations and the influence of paleo-wind patterns with backstepping, aggradational and progradational growth increments. The new model narrows the flank uncertainty by splitting the flank into an upwind and a down-wind side with distinct rock properties. While there are still no direct data from the upwind flank the new model suggests that leeward deposits have been penetrated in cored intervals making it possible to use representative data for the

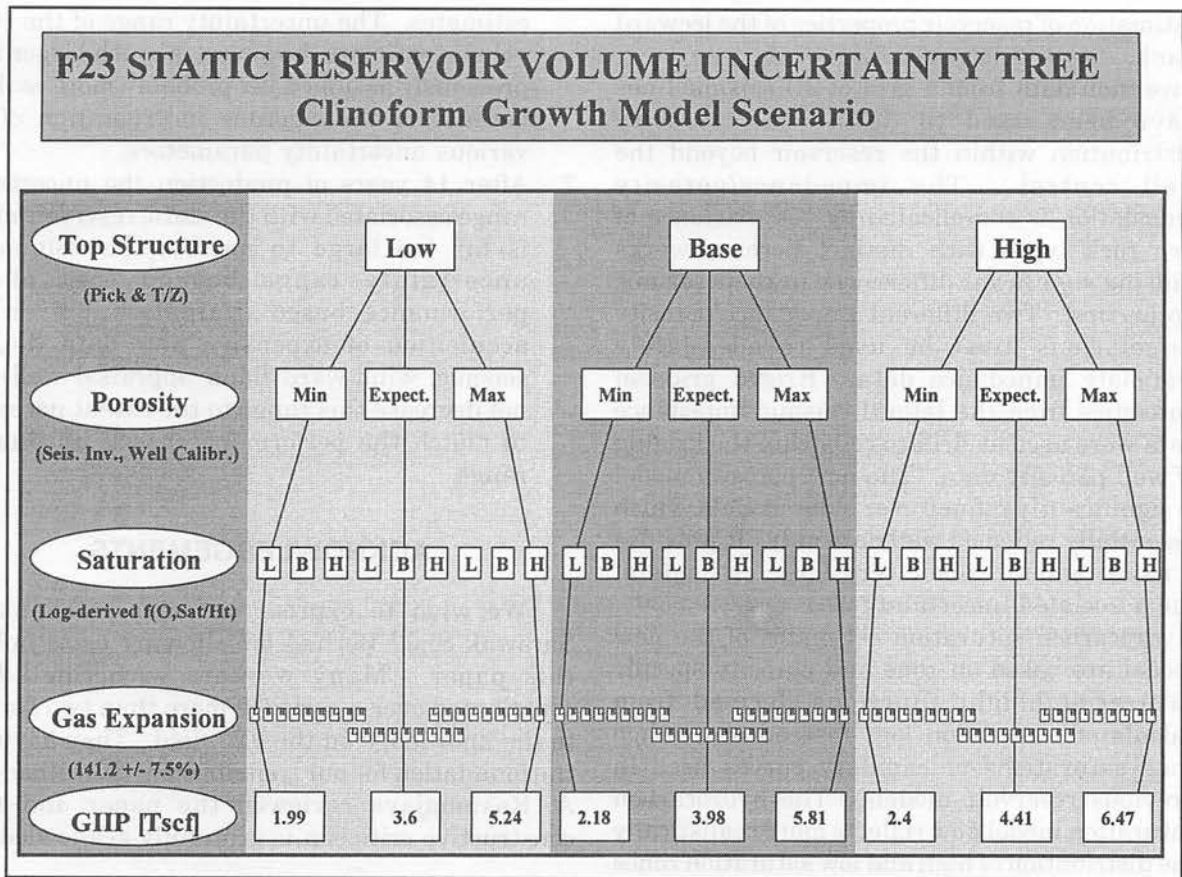


**Figure 5.** Uncertainty tree for the static reservoir volume of F23 field. The geological scenario considered is based on a dynamic model of platform growth with several cycles of backstepping, aggradational and progradational growth periods.

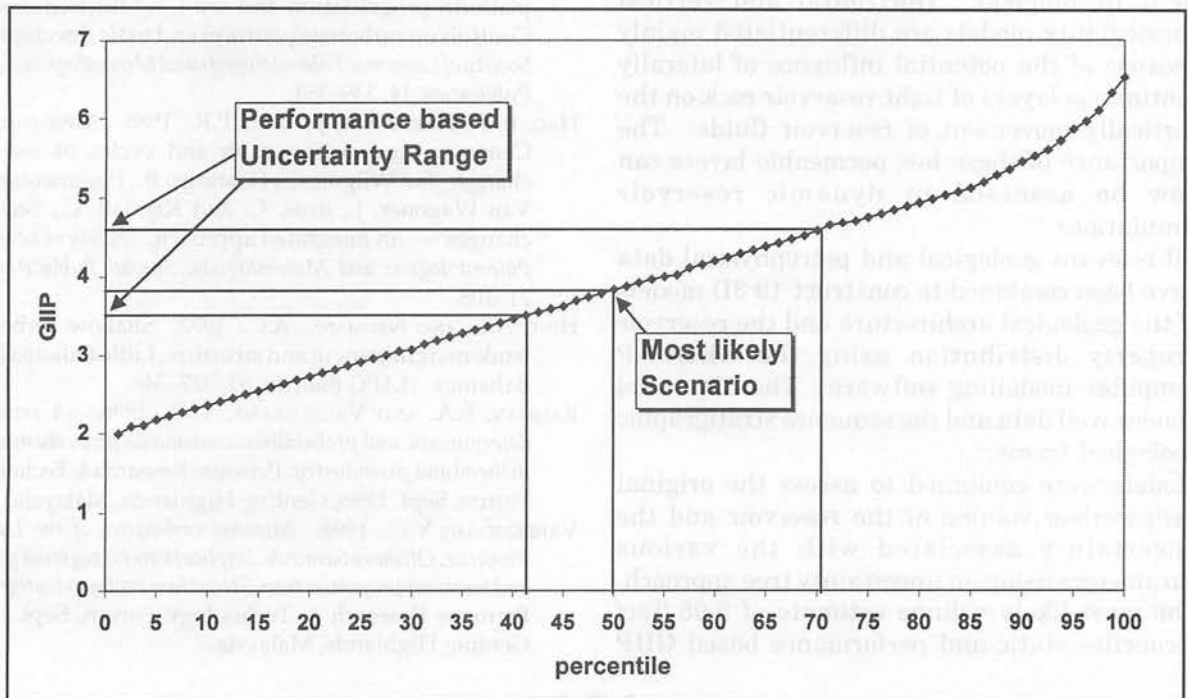


**Figure 6.** Compilation of the GIP volumes from all static model scenarios listed in the uncertainty tree (see Fig. 5). While expectation and most likely volumes are reconciled the performance based GIP uncertainty (after some 14 years of production) is significantly smaller compared to that of the static reservoir model.

- estimation of reservoir properties of the leeward flank.
2. Inversion data from a grid of 2D seismic lines have been used to define the porosity distribution within the reservoir beyond the well control. The impedance/porosity translation is complicated by the existence of two rock types with distinct pore networks causing significant differences in their seismic properties. Two different impedance/porosity correlations must be used to adequately translate impedance data. Kriged grids of porosities from the lateral seismic impedance data were used as drift to constrain the kriging of well porosity data. The new porosity model is significantly refined over older models, which essentially relied on well data only. It provides a more realistic albeit very large estimate of the associated uncertainty.
  3. Hydrocarbon saturation estimates of the new model are based on zone and porosity specific saturation/height functions derived from calculated saturation logs instead of average zone saturations or capillary curves used in previous reservoir models. The hydrocarbon saturation model now reflects more realistically the distribution of high and low saturation zones in the reservoir.
  4. Permeability models have been constructed using porosity/permeability correlations for the three principle rock types (chalky, moldic and tight lithologies). Horizontal and vertical permeability models are differentiated mainly because of the potential influence of laterally continuous layers of tight reservoir rock on the vertically movement of reservoir fluids. The importance of these low permeable layers can now be assessed in dynamic reservoir simulations.
  5. All relevant geological and petrophysical data have been combined to construct 19 3D models of the geological architecture and the reservoir property distribution using the GEOCAP computer modelling software. The 3D model honour well data and the sequence stratigraphic geological frame.
  6. Models were combined to assess the original hydrocarbon volume of the reservoir and the uncertainty associated with the various parameters using an uncertainty tree approach. The most likely volume estimate of 3.98 Tscf reconciles static and performance based GIIP

estimates. The uncertainty range of the static volume estimate, however, is much larger than previously assumed yet probably more realistic because of the rigorous incorporation of the various uncertainty parameters.

7. After 14 years of production the uncertainty range associated with the static reservoir model is far too large to narrow the volumetric uncertainty range beyond that of the performance based evaluation. Even the acquisition of expensive new data (i.e. 3D seismic, wind-ward flank appraisal well) will not decrease this range to the extent necessary to match the performance based uncertainty range.

## ACKNOWLEDGEMENTS

We wish to express our sincere thanks to Sarawak Shell Berhad for allowing us to publish this paper. Many workers with Shell have contributed over a period of more than two decades to the knowledge on the F23 field. They have laid the foundation for our contribution. R. Aalbers and A. Kasumajaya reviewed the paper and their constructive criticism is gratefully acknowledged.

## REFERENCES

- EBERLI, G.P. AND GINSBURG, R.N., 1989. Cenozoic progradation of Northwestern Great Bahama Bank, a record of lateral platform progradation and sea-level fluctuations. *In: Controls on carbonate platform and basic development. Society of Economic Paleontologists and Mineralogists, Special Publication 44*, 339–351.
- HAQ, B.U., HARDENBOL, J., VAIL, P.R., 1988. Mesozoic and Cenozoic chronostratigraph and cycles of sea-level change. *In: Wilgus, C., Hastings, B., Posamentier, H., Van Wagoner, J., Ross, C. and Kendall, C., Sea-level changes — an integrated approach. Society of Economic Paleontologists and Mineralogists, Special Publication 42*, 71–108.
- HINE, A.C. AND NEUMANN, A.C., 1977. Shallow carbonate-bank-margin growth and structure, Little Bahama Bank, Bahamas. *AAPG Bulletin*, 61, 327–348.
- RAHMAN, S.A. AND VAHRENKAMP, V.C., 1996. *A review of deterministic and probabilistic continuous property mapping in the oil and gas industry*. Petronas Research & Technology Forum, Sept. 1996, Genting Highlands, Malaysia.
- VAHRENKAMP, V.C., 1996. *Miocene carbonates of the Luconia Province, Offshore Sarawak: Implications for regional geology and reservoir properties from Strontium-isotope stratigraphy*. Petronas Research & Technology Forum, Sept., 1996, Genting Highlands, Malaysia.